SCIENTIFIC REPORTS
nature research

OPEN

Light transport and vortex-supported wave-guiding in micro-structured optical fibres

Andrey Pryamikov[1*], Grigory Alagashev[2], Gregory Falkovich[3,5] & Sergei Turitsyn[4,5]

In hydrodynamics, vortex generation upon the transition from smooth laminar flows to turbulence is generally accompanied by increased dissipation. However, vortices in the plane can provide transport barriers and decrease losses, as it happens in numerous geophysical, astrophysical flows and in tokamaks. Photon interactions with matter can affect light transport in ways resembling fluid dynamics. Here, we demonstrate significant impact of light vortex formation in micro-structured optical fibres on the energy dissipation. We show possibility of vortex formation in both solid core and hollow core fibres on the zero energy flow lines in the cladding. Through intensive numerical modelling using different independent approaches, we discovered a correlation between appearance of vortices and reduction of light leakage by three orders of magnitude, effectively improving wave guiding. This new effect potentially might have strong impact on numerous practical applications of micro-structured fibres. For instance, a strong light localization based on the same principle can also be achieved in the negative curvature hollow core fibres.

Transverse confinement of a flow is fundamental to many fields of science and technology. Decreasing momentum losses through the pipe walls reduces drag and can save us trillions in the energy cost of oil and gas transport. Decreasing heat losses through tokamak walls is crucial for thermonuclear fusion. Wave guiding of photons in optical fibre is important for optical communications (and Internet), high power lasers, imaging, beam delivery and other optical technologies. In a standard step-index fibre, transversal confinement is ensured by the total internal reflection, but decreasing light leakage is a challenge in micro-structured fibres emerging in a variety of modifications.

Appearance of vortices in a flow can have opposite effects on confinement. In pipe and channel flows, from industrial to cardiovascular systems, generation of vortices generally increases dissipation while vortex suppression can lead to drag reduction. On the contrary, in rotating, magnetized systems and in fluid layers, quasi-two-dimensional vortices have separatrices, serving as transport barriers. Most dramatic example is the transition from low to high confinement in tokamak when zonal vortex flow suppresses heat transfer to the walls. Here we show how generation of optical vortices correlates with significantly improved light confinement in micro-structured fibres. The waveguide losses can be reduced by several orders of magnitude.

Though optics and hydrodynamics look distinct, wave dynamics and underlying mathematical models have many qualitative and quantitative similarities[1–6]. In particular, in nonlinear fibre optics a number of physical effects have been observed, that closely resemble nonlinear hydrodynamic problems, including modulations instability, oceanic rogue waves, localized nonlinear structures, shock waves, optical turbulence[1–13]. These similarities provide possibilities to transfer knowledge and techniques, and observe beautiful and non-evident connections between the two diverse fields. The present work reveals an interesting and potentially highly important connection through the analysis of formation of vortex structures in optical fibres and its impact on the light energy flows.

For quantum and wave phenomena described by a complex field, vortex is an amplitude-zero topological phase defect[1–13]. For instance, an anomalous light transmission through a subwavelength slit in a thin metal plate is accompanied by wave-guiding and phase singularities – vortices of the optical power flow[14]. In nonlinear media, the vortices can exist in the form of topological solitons[15].

[1]Fibre Optics Research Center of Russian Academy of Sciences, Moscow, 119333, Russia. [2]D. Mendeleev University of Chemical Technology of Russia, Moscow, 125047, Russia. [3]Weizmann Institute of Science, Rehovot, 76100, Israel. [4]Aston Institute of Photonic Technologies, Aston University, Birmingham, UK. [5]Aston-Novosibirsk Centre for Photonics, Novosibirsk State University, Novosibirsk, Russia. *email: pryamikov@mail.ru

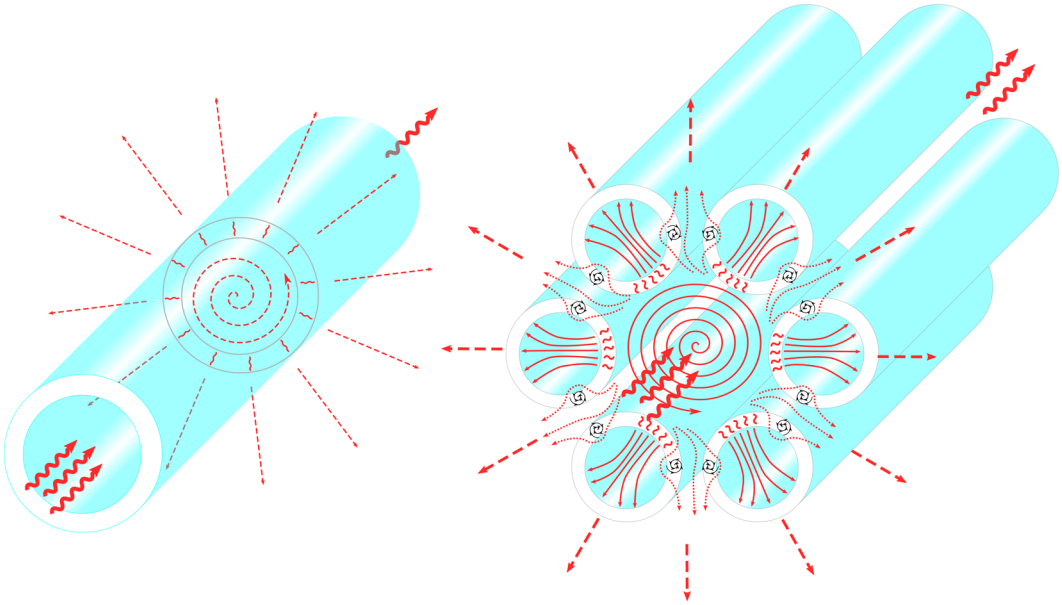

Figure 1. Vortex – supported guidance in micro – structured fibres. (left) Monochromatic radiation in the leaky core mode of the hollow capillary. The axial component of the Poynting vector is from left to right (wavy red arrows). The mode losses are determined by the transverse component of the Poynting vector whose streamlines are represented by dashed red arrows. The losses are high because the streamlines of the transverse component are refracted at the hollow core boundary and further in the empty space are directed radially. (right) Hollow core micro - structured fibre. The streamlines of the transverse component are deviated by the optical vortices in the cladding, where the transverse component of the Poynting vector turns into zero, which leads to loss reduction. (We used Inkscape software to create the image).

Three main features associated with optical vortices (OVs) are zero intensity and phase indefiniteness in the center (phase singularity), and a screw dislocation of the wave front[16,17]. In two dimensions, phase singularities occur when three or more plane waves or two Gaussian pulses interfere and light vanishes at some points[18]. Phase rotates by 2π around the zero-intensity point, which leads to circulation of the optical energy. A circular flow of energy leads to the ability of optical vortices to carry angular momentum (AM).

The classical AM is well studied for the monochromatic waves in free space. In recent years, AM transfer in dielectrics and fibres has attracted much interest[19–24]. To date, the OVs in waveguides have been considered mostly for eigenmodes of step-index or graded-index fibres[25–27]. A systematic study of the internal energy flow of light beams (Gaussian, Laguerre – Gaussian, Bessel) during their propagation in free space was carried out only in few works[28–30]. In this case, singularities of the internal flows occur where the Poynting vector or its transverse component vanishes[29]. In the case of transverse flow fields, the singular points can be nodes, saddle points, vortices, spiral points. In work[30] the Poynting vector singularities were classified based on the theory of dynamic systems as applied to optics. The work described the Poynting vector singularities of both types associated with either the vector field singularities (zeros of the electric and magnetic fields) or mutual polarization of the fields (owing to vector product). In addition, in[31] it was demonstrated that the components of the Poynting vector vary in sign for some phase difference between TE and TM – polarized waves forming Bessel beam.

In this work, we examine for the first time the linear OVs that occur in the cladding of micro-structured optical fibres (MOFs), all solid photonic band gap fibres (ASBGF)[32] and a new type of hollow core fibres - negative curvature hollow core fibres (NCHCF)[33–35]. OVs considered here arise in the transverse component of the Poynting vector of the core modes, which determines the losses of these modes in the micro-structured fibres. The process of energy leakage from the fiber core can be most clearly represented by the energy flow lines or streamlines of the transverse component of the Poynting vector of the core modes[36]. The transverse component of the Poynting vector always has an uncertainty in direction and zero value at the origin. The novelty of our work is in the analysis of the singularities of the transverse component of the Poynting vector of the core modes of micro-structured optical fibers and in correlating their formation with the level of fibre losses. We have demonstrated that by changing the geometric parameters of such fibers, one can find such a configuration of vortex structures in the fiber cladding that can lead to a significant reduction of leakage losses.

Summary of Results

The main result of our work is the discovery and quantitative analysis of the correlation between formation of optical vortices and fibre leakage losses. Waveguide microstructures with continuous rotational symmetry of the core-cladding boundary, such as dielectric tube waveguides or Bragg fibers, have no singularities (OVs) in the energy flow lines of the core modes in the cladding (Fig. 1(left)). The singular points of the transverse Poynting vector component occur in MOFs with discrete rotational symmetry of the cladding elements such as ASBGFs or NCHCFs. Discrete rotational symmetry of the cladding elements arrangement in the MOFs defines the azimuthal

energy fluxes of the core modes. This energy flux leads to the formation of additional vortices both inside the cladding elements and in the space between them (Fig. 1(right)). As stated in[29], the vortices 'organize' the whole field in the neighboring space. The phase dislocations in the electromagnetic wave structure in free space occur when the real and imaginary parts of the field strength are simultaneously equal to zero[37]. The stream lines of the transverse Poynting vector $\overrightarrow{P_{transv}}$ of the core modes in a cross section of the graded - index fibre are described by the equations $dx/P_x(x,y) = dy/P_y(x,y)$, where P_x and P_y are the components of $\overrightarrow{P_{transv}}$. The locations of the OVs in the streamlines are determined by the condition $P_x(x,y) = P_y(x,y) = 0$[38]. We demonstrate here that these conditions define the positions of the OV centers in the cladding of ASBGFs and NCHCFs. Also, we demonstrate OV induced wave-guiding effect, in which photons passing through the optical fibre excite the circulating power currents that impact light transport and decrease the overall losses. This reduction in losses is achieved due to the "negative propagation" of the leaky light energy[29,31] (backward propagation of the core mode leaky energy). The formation of the OV in the cladding capillary walls of silica glass NCHCFs leads to a strong light localization in the hollow core, which makes it possible to transmit radiation in the mid IR spectral range[39].

Vortex – Supported Wave - Guiding in all Solid Band Gap Fibres

Dislocations of monochromatic waves are stationary in space and form isolated interference fringes. The phase of the field is undefined on the zero-amplitude lines and changes by π when crossing them. The wave front dislocations of coherent radiation can be characterized by zero field amplitude in its center or along the dark rings where the field amplitude vanishes. The origin of the dark rings and dislocation centers is boundary diffraction and destructive interference.

For such micro – structured optical fibres as ASBGFs or NCHCFs the electric and magnetic fields of the core modes $\overrightarrow{E}(r,\ \phi)e^{i(\beta z-\omega t)}$ and $\overrightarrow{H}(r,\ \phi)e^{i(\beta z-\omega t)}$ can be described by specifying the axial components of the fields E_z and H_z, where ω denotes the angular frequency and β is propagation constant of the core mode. Then, the wave equation for each axial component is the Helmholtz equation:

$$\overrightarrow{\nabla}^2 F + k_t F = 0,$$

where $F = E_z$ or $F = H_z$ and $k_t = \sqrt{k_0^2 n_i^2 - \beta^2}$ is the transverse component of the wavevector, $k_0 = 2\pi/\lambda$ and n_i is a refractive index of the cladding element or surrounding area. In the case of micro - structured fibres it is possible to separate the "longitudinal" phase of the core mode $e^{i\beta z}$ and the "transversal" phase.

Each component of the core mode fields in the vicinity of the cladding element is a linear superposition of an infinite set of cylindrical harmonics. Axial components of the fields can be expressed as:[40]

$$E_z = \sum_{m=-\infty}^{+\infty} A_m F_m(k_t r) e^{im\phi}, \qquad (1)$$

$$H_z = \sum_{m=-\infty}^{+\infty} B_m F_m(k_t r) e^{im\phi},$$

where $F_m(r)$ is Bessel function of 1th order if $r < a$ and Hankel function of 1th order if $r > a$, a is the radius of the cladding dielectric cylinder. For Hankel function of 1th order the radiation condition at infinity is satisfied.

All transversal components of the core mode fields can be expressed in terms of the axial component using well known relations[41]. For example, azimuthal components of the core mode fields are:

$$E_\phi = \frac{i}{k_t^2}\left(\frac{\beta}{r}\frac{\partial E_z}{\partial \phi} - k_0 \frac{\partial H_z}{\partial r}\right), \qquad (2)$$

$$H_\phi = \frac{i}{k_t^2}\left(\frac{\beta}{r}\frac{\partial H_z}{\partial \phi} + k_0 n_i^2 \frac{\partial E_z}{\partial r}\right).$$

The details of calculation of the expansion coefficients of the cylindrical harmonics in (1) and the complex propagation constants of the core modes performed using the Multipole method can be found in[40] and in the section Methods. In addition, we performed the same calculations using COMSOL 4.4 software package. Part of the figures and calculations in the paper were also made using COMSOL 4.4.

We considered all solid band gap fibres with one and two rows of the cladding dielectric rods. The refractive index contrast between the cladding rods and the surrounding glass matrix ($n_{glass} = 1.45$) is $\Delta n = 0.05$. The arrangement of the rods has a hexagonal structure. The value of a pitch of $\Lambda = 12\,\mu m$ (distance between the centers of the cladding rods), and the ratio of $d/\Lambda = 0.33$, where d is the cladding rod diameter.

Let us consider the light leakage from the fibre core and calculate the loss dependencies on the wavelength for the fundamental core mode in several transmission bands. The loss dependencies on the wavelength for both ASBGFs are shown in Fig. 2 and have several transmission bands according to the band gap waveguide mechanism[32]. It is seen that there are relatively narrow transmission bands in which the losses are three orders of magnitude lower than in the rest of the spectrum.

This is especially true for the fibres with one row of the cladding rods. The same resonant loss reduction can be observed if we fix the wavelength, for example, in the minimum of losses at a wavelength of $\lambda = 1\,\mu m$, and change the value of the pitch Λ. The calculation results are shown in Fig. 3. As in Fig. 2, there is a sharp decrease in losses

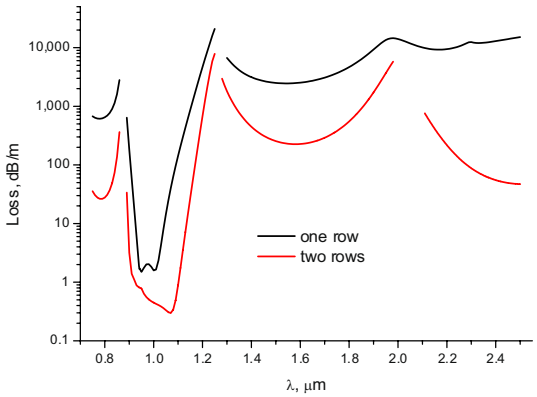

Figure 2. Loss dependence of the fundamental core mode on the wavelength for all solid band gap fibres with one (black) and two rows (red) of the cladding rods. The geometrical and material parameters of the fibres are in the text.

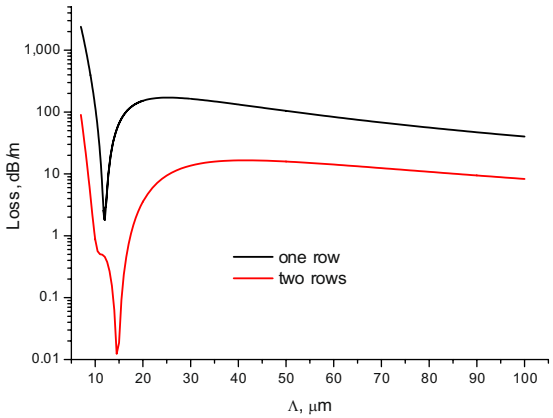

Figure 3. The loss dependencies of the fundamental core mode on the value of the pitch for all solid band gap fibres described in the text. The black curve for one row, the red curve for two rows of the cladding rods.

by several orders of magnitude in both cases in a narrow range of the pitch values. It is clear that this substantial decrease in losses for both fibres can be only associated with the narrow spectral regions and with specific values of the pitch.

Light leakage of the core modes can be characterized by the distribution of projection of the transverse component of the Poynting vector on the radius - vector drawn from the origin P_r. The values of the projection of the transverse component of the Poynting vector for the fundamental core mode were calculated at the wavelengths of $\lambda = 1\,\mu m$, $1.5\,\mu m$ and a value of pitch of $\Lambda = 12\,\mu m$ (Fig. 2).

As in the case of polygonal waveguides[42], the distribution of the radial component of the the transverse Poynting vector has periodic alternating character, which points to a vortex structure of the core mode fields in the cladding (Fig. 4). The vortex structures for both distributions of the radial projection of the transverse component of the Poynting vector are different at different wavelengths (Fig. 4). In the case of minimal losses (Fig. 4(left)), the OVs centers are located inside the cladding rods, while in the case of large losses (Fig. 4(right)), the OVs are located at the boundaries of the cladding rods. Thus, the leaky radiation of the fundamental core mode moves along different trajectories in the cladding. The "negative propagation" of leaky energy of the core mode implies some balance between the mode energy flowing from the core and the energy flowing back into the core. The magnitude of this energy balance determines the losses in the waveguide. It is well established that the single fundamental property of the optical vortex formation is the rotation of the Poynting vector (energy rotation) around the phase dislocation (the OV core)[16,17].

To clearly demonstrate the OV formation and the formation of phase dislocations of various structures in the cladding of the all solid band gap fibre with one ring of the cladding rods (Fig. 4) let us consider the distribution of the stream lines of the transverse Poynting vector component of the fundamental core mode $\overrightarrow{P}_{transv}$ and the lines of zero components of $\overrightarrow{P}_{transv}(x, y) = \left\{P_x(x, y) = 0;\, P_y(x, y) = 0\right\}$ at wavelengths of $\lambda = 1\,\mu m$ and $\lambda = 1.5\,\mu m$ (Fig. 2). The distribution for the wavelength of $\lambda = 1\,\mu m$ is shown in Fig. 5.

The structure of the Poynting vector streamlines shown in Fig. 5 points to the formation of the dislocation lines around which the leaky radiation of the fundamental core mode rotates. The vortex centers are formed at the intersection points of the curves $P_x(x, y) = 0$ and $P_y(x, y) = 0$. Moreover, it can be seen from Fig. 5 that there are

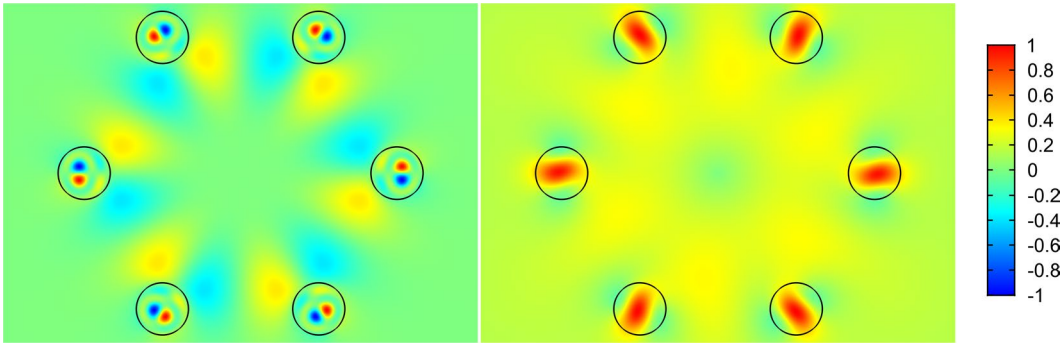

Figure 4. The map of the radial component of the Poynting vector for all solid band gap fibres with one row of rods ($\Lambda = 12\,\mu m$). (left) $\lambda = 1\,\mu m$ (Fig. 2); (right) $\lambda = 1.5\,\mu m$ (Fig. 2). (We used COMSOL Multiphysics v.4.4. www.comsol.com. software to create the image).

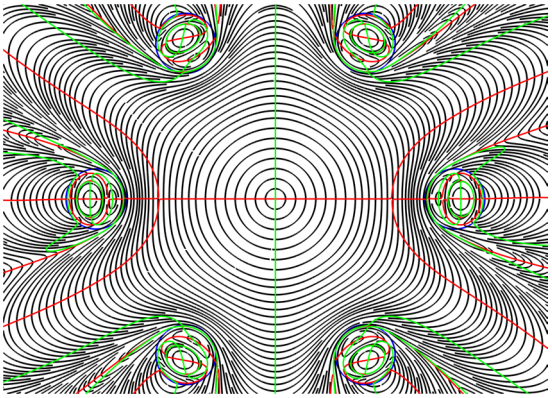

Figure 5. The streamlines of the transverse component of the Poynting vector (grey lines) and the lines of zero intensity $\overrightarrow{P_{transv}} = \{P_x = 0;\ P_y = 0\}$ ($P_x = 0$ (red lines), $P_y = 0$ (green lines)) for all solid band gap fibre with a cross section shown in Fig. 4 at a wavelength of $\lambda = 1\,\mu m$. (We used COMSOL Multiphysics v.4.4. www.comsol.com. software to create the image).

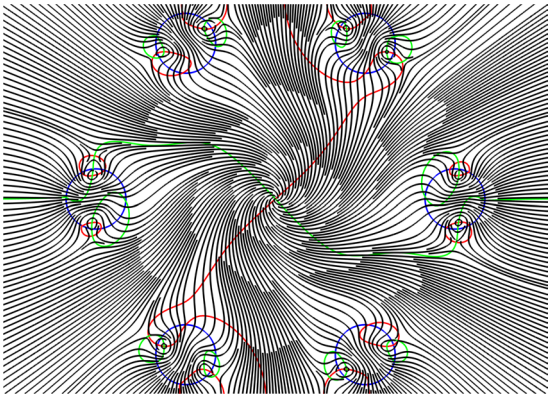

Figure 6. The streamlines of the transverse component of the Poynting vector (grey lines) and the zero lines $\overrightarrow{P_{transv}} = \{P_x = 0;\ P_y = 0\}$ ($P_x = 0$ (red lines), $P_y = 0$ (green lines)) for all solid band gap fibre with a cross section shown in Fig. 4 at a wavelength of $\lambda = 1.5\,\mu m$. (We used COMSOL Multiphysics v.4.4. www.comsol.com. software to create the image).

closed areas, where light rotates around the dislocation lines. In addition, there are areas of the cladding where the two curves are very close to each other and form the ring phase dislocations inside the rods[43].

Although the streamlines distribution of the transverse component of the Poynting vector at a wavelength of $\lambda = 1.5\,\mu m$ forms the OVs (Fig. 6), the energy of the core mode efficiently flows through different paths in the cladding and rotates only in small regions near the OV centers at the rod boundaries. Moreover, a major part of

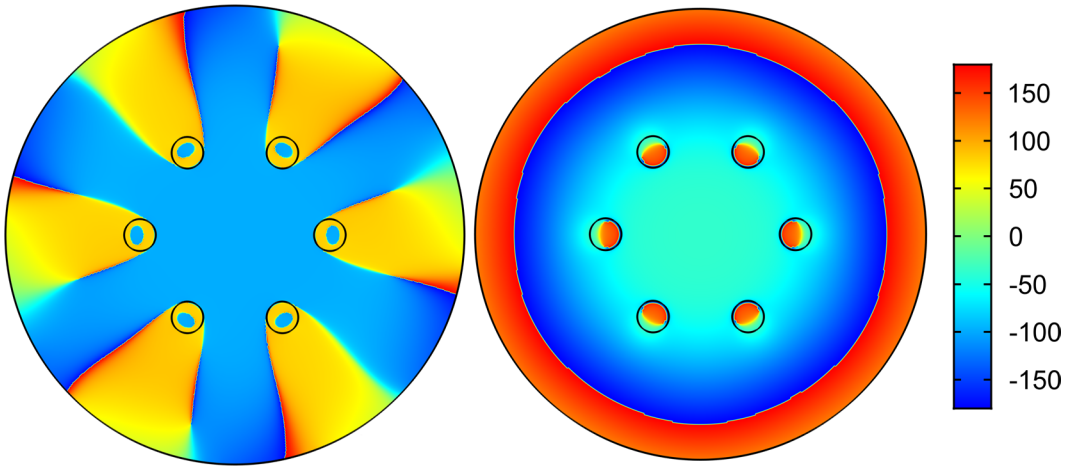

Figure 7. (left) the phase distribution of the transverse electric field component E_x for the fundamental core mode of ASBGF with one row of the cladding rods at a wavelength of $\lambda = 1\,\mu m$; (right) the phase distribution of the transverse electric field component E_x for the fundamental core mode of ASBGF with one row of the cladding rods at a wavelength of $\lambda = 1.5\,\mu m$. (We used COMSOL Multiphysics v.4.4. www.comsol.com. software to create the image).

the core mode radiation flows through the cladding rods (Fig. 4(right)) which, in contrast to the previous case, cannot serve as effective reflectors for the leaky radiation. This leads to large losses in the fibre (Fig. 2 and Fig. 4).

Let us now consider the phase distribution of the transverse component of core mode electric field, for example, E_x. According to the general principles of the optical vortices theory[16,17], the phase distribution of the transverse component of the core mode electric field should experience a jump in π when passing through the boundary of the closed area around the dislocation lines. We calculated the phase distribution of E_x in the cladding of both fibres for two wavelengths of $\lambda = 1\,\mu m$ and $\lambda = 1.5\,\mu m$ (Fig. 2).

The phase distribution of E_x for the fibre with one row of the cladding rods is shown in Fig. 7. The vertical scale represents the phase values in degrees. It can be seen from Fig. 7(left) that the OVs located in the cladding rods at wavelength of $\lambda = 1\,\mu m$ have a corresponding phase jump π for the distribution of E_x. The phase distribution of E_x at a wavelength of $\lambda = 1.5\,\mu m$ has a qualitatively different character Fig. 7(right). In this case, the phase distribution does not experience a pronounced jump in π in the cladding rods, so the ring phase dislocations for the fundamental core mode don't form in the cladding rods. This difference in the core mode field structure leads to a difference in the loss level at these two wavelengths. It is possible to demonstrate that in the case of ASBGFs with two rows of the cladding rods (Figs. 2, 3) the loss reduction is also determined by the phase ring dislocations in the rods.

Figures 5, 6 demonstrate qualitative (topological) difference between two cases. Only isolated vortices exist for $\lambda = 1.5$, which makes the energy to spiral out without returning. On the contrary, the green and red lines in Fig. 5 cross not only at isolated points but also coincide along the whole radial lines, which are thus vortex lines having phase jump in the left panel of Fig. 7. Those vortex lines provide for energy recirculation and improved confinement at wavelength of $\lambda = 1\,\mu m$.

Vortex – Supported Wave - Guiding in the Negative Curvature Hollow Core Fibres

To demonstrate the vortex - supported wave – guiding in the NCHCFs and its distinction from the wave – guiding in waveguides with continuous rotational symmetry of the core – cladding boundary, let us consider the loss dependence of the fundamental air core mode on the wavelength for three waveguide micro - structures.

The first one is a single capillary with a wall thickness of 0.65 μm and the air core diameter of 14.4 μm. The refractive index of the capillary wall is equal to 1.5 as in the case of ASBGF considered in Section 2.

The second one is a waveguide consisting of two capillaries nested in one another and having a common center. The internal capillary has the same parameters as the single capillary described above. The outer capillary has an inner diameter of 32.3 μm and the same wall thickness as the internal capillary. The light localization in both waveguides can be described within the ARROW model[44]. The capillary wall can be considered as Fabry – Perrot resonator which either passes radiation outside (condition of the resonant regime is $k_t d = \pi m$, where k_t is the transverse component of the air core mode wavevector, d is the capillary wall thickness and m is an integer) or reflects it into the air core (condition of the anti – resonant regime is $k_t d = \pi(m + 1/2)$). In this case, the losses are consequently reduced with the addition of each new cladding layer (Fig. 8). The NCHCF has 6 cladding capillaries with a wall thickness of 0.65 μm, the inner diameter of 8.3 μm and the air core diameter is 14.4 μm. The distance between the nearest points of the adjacent cladding capillaries is 2.4 μm.

The losses of NCHCF with 6 cladding capillaries are approximately two orders of magnitude lower than in the double capillary fibre at the point of minimum loss (Fig. 8). This difference in losses can be explained by the difference in the leakage process for the fundamental air core mode between these cases. Another dissimilarity pertains to the loss behavior of the NCHCF at the long wavelength edge of the short wavelength transmission

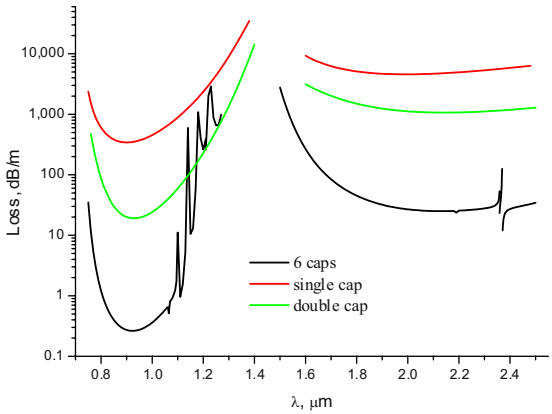

Figure 8. Loss dependence of the fundamental air core mode on the wavelength for three waveguide microstructures: NCHCF with 6 capillaries in the cladding (black), a single capillary waveguide (red) and a double capillary waveguide (green).

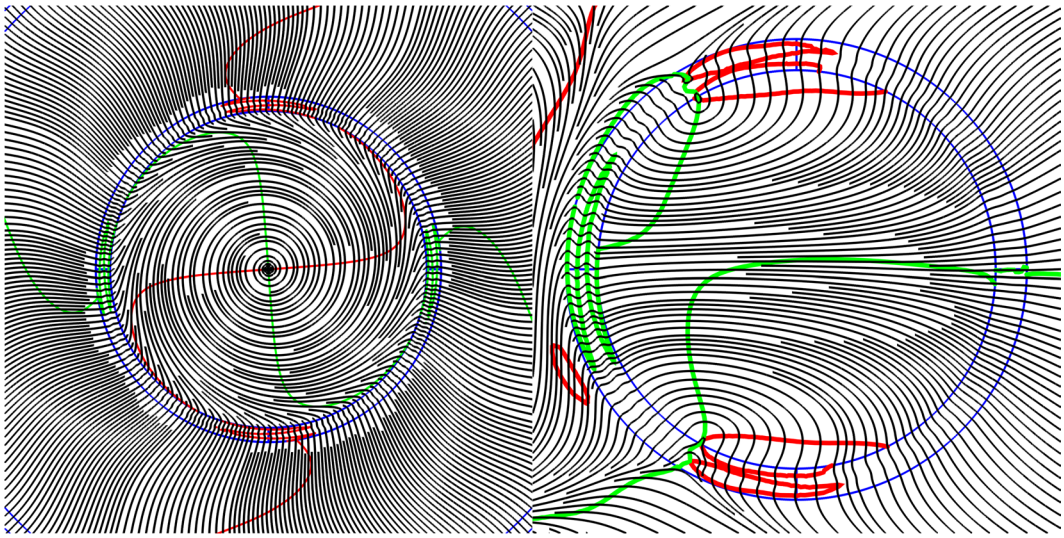

Figure 9. Streamlines of the transverse component of the Poynting vector (grey) of the fundamental core mode and its zero lines $P_x = 0$ (red lines), $P_y = 0$ (green lines)) for the internal capillary of the double capillary fibre (left) and (right) for the single cladding capillary of NCHCF with 6 cladding capillaries at a wavelength of $\lambda = 0.9\,\mu m$ (Fig. 8). (We used COMSOL Multiphysics v.4.4. www.comsol.com. software to create the image).

band (Fig. 8) and originates from the coupling between the fundamental air core and the cladding modes with a certain type of discrete rotational symmetry[45].

As in the case of ASBGFs, the leakage process for the fundamental air core mode can be characterized by the streamlines of the transverse component of the Poynting vector and the lines of zero components of $\overrightarrow{P_{transv}} = \{P_x(x, y) = 0; P_y(x, y) = 0\}$. The corresponding distribution of the streamlines of $\overrightarrow{P_{transv}}$ and the points of intersection of $P_x(x, y) = 0$ and $P_y(x, y) = 0$ are shown in Fig. 9 for the internal capillary of the double capillary fibre and the single cladding capillary of the NCHCF whose losses are shown in Fig. 8. The calculations were carried out at the center of the second transmission band at a wavelength of $\lambda = 0.9\,\mu m$ (Fig. 8). It can be seen from Fig. 9 (left) that the curves $P_x(x, y) = 0$ and $P_y(x, y) = 0$ have no intersection points in the case of the double capillary waveguide.

Thus, the OV formation in the capillary wall is impossible. It was shown in[42] that in this case the radial projection of the transverse component of the Poynting vector P_r must be positive along the whole core – cladding boundary of the capillary. For the double capillary fibre this distribution is shown in Fig. 10 for the sum of two orthogonally polarized fundamental air core modes. In all points of the cladding, $P_r > 0$ and streamlines are directed along the radial direction only. The magnitude of P_r is normalized by the value of the axial component of the Poynting vector for the sum of two orthogonally polarized fundamental air core modes, which is taken to be one watt. The distribution of P_r does not depend at all on the azimuthal angle φ along any circle.

A different situation is observed in the case of the NCHCFs. The OVs centers are formed at the intersection points of the curves $P_x(x, y) = 0$ and $P_y(x, y) = 0$, where the distance between the cladding capillaries is minimal

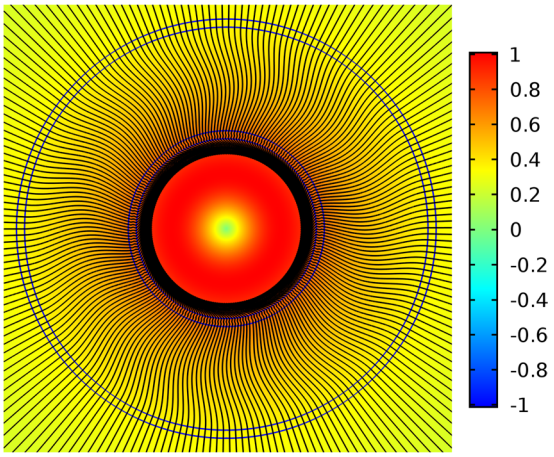

Figure 10. The distribution of projection of the transverse component of the Poynting vector on the radius – vector drawn from the origin for the double capillary fibre at a wavelength of $\lambda = 0.9\,\mu m$ (Fig. 8). The streamlines of the transverse component of the Poynting vector of the fundamental air core mode are shown in black. (We used COMSOL Multiphysics v.4.4. www.comsol.com. software to create the image).

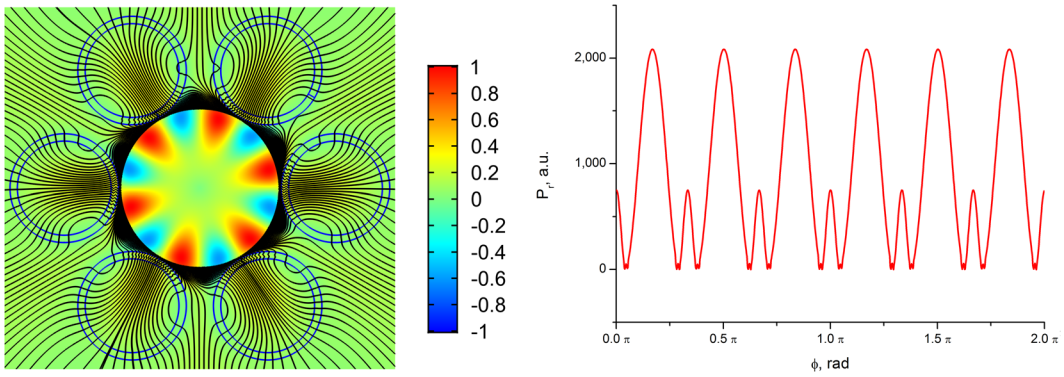

Figure 11. (left) The distribution of projection of the transverse component of the Poynting vector on the radius – vector drawn from the origin for NCHCF with 6 cladding capillaries and streamlines of the transverse component of the Poynting vector (black lines) at a wavelength of $\lambda = 0.9\,\mu m$ (Fig. 8); (right) the distribution of this projection on azimuthal angle φ along the circle with a radius of $R = 10.6\,\mu m$. (We used COMSOL Multiphysics v.4.4. www.comsol.com. software to create the image).

(Fig. 9(right)). They occur both at the boundary and inside the capillary wall. The energy flow of the fundamental air core mode rotates around the vortices. As in the case of the ASBGFs (Fig. 4), some part of the core mode energy flux changes its direction in the regions between the cladding capillaries and then returns to the air core of NCHCF. To confirm this assumption, let us consider a distribution of P_r at the wavelength 0.9 μm, as shown in Fig. 11(left).

It can be seen from Fig. 11(left) that due to the OVs in the cladding capillary walls there are regions between the capillaries, where $P_r = 0$ or $P_r < 0$. Because of these vortices, the energy of the fundamental air core mode passes only through the limited segments of the cladding capillary wall surfaces, which are located closest to the center of the core. Only a small part of this energy passes through the space between the cladding capillaries. In addition, since $P_r < 0$ in separate areas of the space between the cladding capillaries, the fundamental core energy undergoes 'negative propagation'[29,31] back to the fibre core (Fig. 11 (left)). To confirm this conclusion, let us consider the dependence of P_r on the azimuthal angle φ along the circle with the radius 10.6 μm passing near the centers of the OVs (Fig. 11(right)). It can be seen from Fig. 11(right) that the distribution and value of P_r are largely determined by the OV locations in the cladding. Radiation leakage from the NCHCF also occurs in the anti – resonant regime at $\lambda = 0.9\,\mu m$. The normalization of P_r is as in the case of the double capillary fibre.

That regime of light localization was called the local ARROW mechanism (only a limited part of the capillary wall reflects light in the anti – resonant regime)[46].

In the recent paper[47], using technique of transverse power flow streamlines visualization for the air core modes of the negative curvature hollow core fibres[36], it was demonstrated a possibility of reducing losses with only a modest increase in fabrication complexity. When approaching the resonant condition for the cladding elements, for example, at $\lambda = 0.75\,\mu m$ (Fig. 8), the cladding capillary walls become more transparent for the outgoing

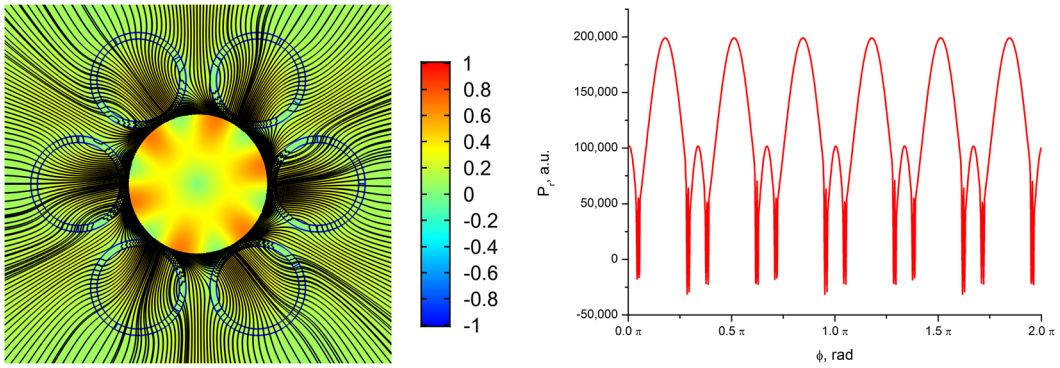

Figure 12. (left) The distribution of projection of the transverse component of the Poynting vector on the radius – vector drawn from the origin for NCHCF with 6 cladding capillaries and streamlines of the transverse component of the Poynting vector (black lines) at a wavelength of $\lambda = 0.75\,\mu m$ (Fig. 8); (right) the distribution of this projection on azimuthal angle φ along the circle with a radius of $R = 10.6\,\mu m$. (We used COMSOL Multiphysics v.4.4. www.comsol.com. software to create the image).

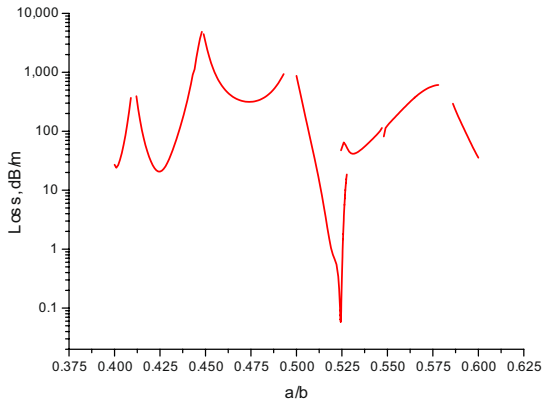

Figure 13. The loss dependence on the ratio of the minor axis to the major axis (a/b) of the cladding capillary for the hollow core fibre with the cladding consisting of 12 ellipsoidal capillaries. The parameters of the fibre are described in the text.

radiation, and the total loss level increases (Fig. 12). Due to the presence of the OVs and the reflective properties of the cladding capillaries, this increase in losses is not significant compared to the increase in losses for the double capillary fibre (Figs. 8, 10). In that case, the vortex structure of $\overrightarrow{P_{transv}}$ is preserved, which leads to an inhomogeneous distribution of the outgoing energy flux depending on the azimuthal angle and reduces the leakage loss growth (Fig. 12(right)).

The geometrical parameters of both NCHCFs and ASBGFs have a strong impact on the OV formation in the cladding at a given wavelength and, consequently, on wave – guide properties of the micro – structured fibres. By changing the distance between the walls of adjacent cladding capillaries, the number of the capillaries in the cladding or the distance between their centers, it is possible to control the positions of the vortices in the cladding and the level of light localization in the air core[42]. Moreover, as it was shown in[36], the introduction of the supporting tube does not significantly change the vortex formation mechanism in NCHCFs.

In order to demonstrate the influence of the geometric parameters of the cladding elements on the loss level of the fundamental core mode in waveguides with a complex cladding structure, we considered a hollow core fibre with a cladding consisiting of 12 ellipsoidal capillaries. We calculated the dependence of the fundamental mode loss on the ratio of the minor axis to the major axis of the ellipsoidal cladding element (a/b). The magnitude of the major axis was $8.3\,\mu m$, the wall thickness of the ellipse was $0.65\,\mu m$, and the hollow core of the waveguide was $R_{core} = 14\,\mu m$. The refractive index of the wall of the ellipsoidal capillary was $n = 1.5$ as in previous cases. The results of the calculation at $\lambda = 1\,\mu m$ are shown in Fig. 13.

As can be seen from Fig. 13, the waveguide losses of the hollow core fibre described above are high in a wide range of parameter a/b values and only in a narrow region near a/b~0.524 there is a sharp decrease in losses by several orders of magnitude.

In order to demonstrate a qualitative difference in the behavior of the transverse Poynting vector component of the leaky fundamental air core mode, we consider the distribution of the streamlines of the vector and its radial component (in color as in Fig. 4). The corresponding distributions are shown in Fig. 14.

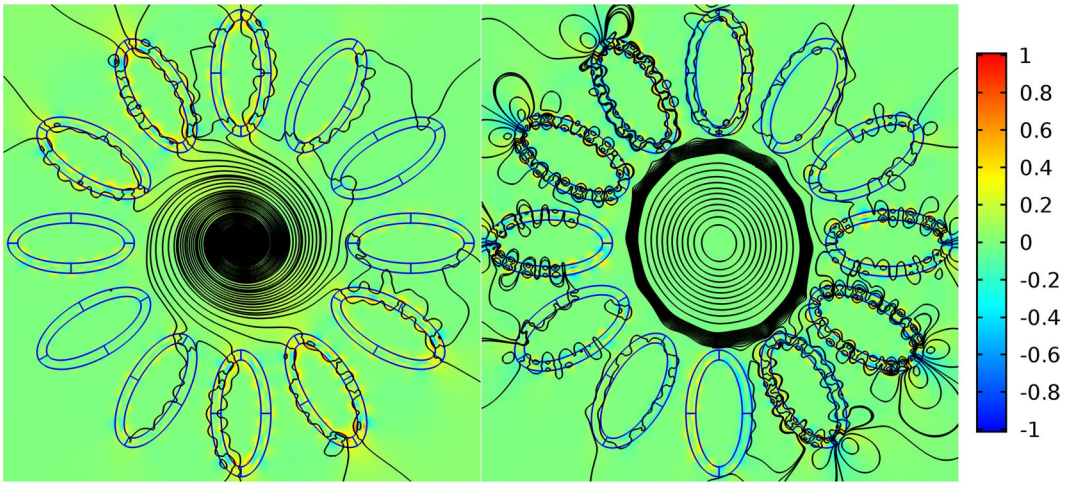

Figure 14. The streamlines of the transverse component of the Poynting vector of the fundamental air core mode for the hollow core fibre with 12 ellipsoidal cladding capillaries. The parameters of the fibre are described in the text. The densities of the streamlines are the same on both panels: left ($a/b = 0.474$) and right ($a/b = 0.524$) (Fig. 13). The distribution of the radial component of the Poynting vector is shown in color. (We used COMSOL Multiphysics v.4.4. www.comsol.com. software to create the image).

It is seen from Fig. 14 that in the case of large losses of the air core mode the streamlines density is much higher in the air core than in the cladding ellipsoidal capillaries, and the color of the radial component of the Poynting vector indicates the flow of the core mode energy through these capillaries into the outer space. Strong leakage of the energy occurs despite the presence of a certain vortex structure in the cladding capillaries (Fig. 14(left)). At the same time, a small change in the parameter a/b makes it possible to reduce losses by three orders of magnitude while changing the vortex structure of the transverse Poynting vector component in the cladding. In this case, the density of the flow lines is much higher precisely in the ellipsoidal capillary wall where the vortices occur than in the air core of the fibre (Fig. 14(right)).

Conclusion

We have studied impact of transversal light vortex formation on energy leakage in micro-structured optical fibres. To the best of our knowledge, it is the first demonstration that creation of a specific configuration of vortices at the intersections of zero energy flow lines can reduce losses by three orders of magnitude. This new effect was verified by two independent methods. Appearance of vortices suppresses light leakage, effectively improving wave-guiding. Depending on the type of rotational symmetry of the arrangement of the cladding elements, minimal losses are achieved when centers of the phase dislocations are located in the cladding element wall. The same underlying physical mechanism provides for a strong light localization in the negative curvature hollow core fibres. The key point of this general concept is that the right arrangement of vortices in the fibre cladding produces a balance between the outward and inward energy flux of the core mode. We anticipate that this mechanism can be used to develop advanced low- loss fibres across spectral range for various applications, from telecom to high power lasers and optical beam delivery.

Methods

To describe vortex formation in the transverse component of the Poynting vector of the leaky core modes of micro-structured optical fibres, we employed two computational methods accounting for all electric and magnetic components of the core mode fields and their complex propagation constants. First, we used a multipole expansion method to perform full-vector modal calculations of the micro-structured optical fibres with circular rods or capillaries in the cladding. This is an efficient approach for micro-structured fibres with circular cladding elements. For a given time dependence is $exp(-i\omega t)$, the core mode fields are expressed via cylindrical harmonics. In the neighborhood of the circular cladding element, the axial components are presented using local cylindrical coordinates (r_i, φ_i), where i is a number of the circular cladding element. In the case of the cladding rods, the axial field components can be expressed in terms of Bessel functions of the first kind (J_m) inside the rod. In the case of the cladding capillary,, the axial components present the sum of Hankel functions of the first and second kind ($H_m^{(1)}$ and $H_m^{(2)}$) in the capillary wall and Bessel functions of the first kind (J_m) in the capillary hollow core. Matching the boundary conditions for radial and azimuthal components of the core mode fields in two domains leads to a matrix equation. It should be noted that the source-free J_m parts of the expansion in the neighborhood of the cladding rod or the capillary i are due to $H_m^{(1)}$ fields radiated from the cladding rods or capillaries $j \neq i$, and in order to obtain the matrix equation when applying the boundary conditions it is necessary to use Graf's addition theorem. The determinant of the matrix defines the propagation constants of the core modes β, and the associated null vectors determine the modal fields. We cross-check the results of our calculations of the propagation constants of the leaky core modes using a commercial software package COMSOL Multiphysics based on finite element method (FEM). The complex propagation constants and distribution of the fields of the leaky core modes have been found by solving the eigenvalue problem for the wave equation for the two types of the micro-structured fibres. The waveguide losses have been calculated

through the imaginary parts of the propagation constant of the fundamental core mode by the above two methods for different geometrical parameters of the fibre and the wavelengths. Further, using the calculated values of the core mode fields, we computed the distribution of the transverse component of the Poynting vector and its stream lines. The positions of the optical vortices in the cross – section of the micro – structured fibre were determined from the equation for the streamlines of the transverse component of the Poynting vector of the core mode $dx/P_x = dy/P_y$. The conditions $P_x(x, y) = P_y(x, y) = 0$ defined the singular points and lines of the streamline pattern in the cross section of the fibre. Optical vortices have been detected in the regions and individual points, where the lines of zero values of transverse Poynting vector components overlap or intersect. The analysis of the vortex distributions and loss dependencies allows us to identify us the connection between the structure of the vortices and the minimum loss values in the micro-structured fibres.

Received: 25 September 2019; Accepted: 30 January 2020;
Published online: 13 February 2020

References

1. Nye, J. F. & Berry, M. V. Dislocations in wave trains. *Proc. R. Soc. Lond. A* **336**, 165–190 (1974).
2. Berry, M. V. Quantal phase factors accompanying adiabatic changes. *Proc. Roy. Soc. Lond. A* **392**, 45–57 (1984).
3. Desyatnikov, A. S., Torner, L. & Kivshar, Y. Optical Vortices and Vortex solitons. *Prog. Opt.* **47**, 291–333 (2005).
4. Falkovich, G. Fluid Mechanics, second edition. (Cambridge University Press. 2018).
5. Pismen, L.M. Vortices in Nonlinear Fields (Clarendon Press 1999).
6. Dudley, J. M., Genty, G., Mussot, A., Chabchoub, A. & Dias, F. Rogue waves and analogies in optics and oceanography. *Nature Reviews Physics* **1**, 675–689 (2019).
7. Chabchoub, A., Hoffman, N., Onorato, M., Dudley, J. M. & Akhmediev, N. Hydrodynamic Supercontinuum. *Phys. Rev. Lett.* **111**, 054104 (2013).
8. Chabchoub, A. *et al*. The nonlinear Schrödinger equation and the propagation of weakly nonlinear waves in optical fibres and on the water surface. *Annals of Physics* **361**, 490–500 (2015).
9. Wetzel, B., Pasquazi, A. & Morandotti, R. Water Waves in Optical Fibres. *Physics.* **7**, 48 (2014).
10. Fatome, J., Finot, C., Millot, G., Armaroli, A. & Trillo, S. Observation of Optical Undular Bores in Multiple Four-Wave Mixing. *Phys. Rev. X* **4**, 021022 (2014).
11. Kodama, Y. & Wabnitz, S. Analytical Theory of Guiding Center Nonreturn-to-Zero Signal Transmission in Normally Dispersive Nonlinear Optical Fibres. *Opt. Letters* **20**, 2291 (1995).
12. Turitsyna, E. G. *et al*. S. K. The laminar-turbulent transition in a fibre laser. *Nature Photon.* **7**, 783–786 (2013).
13. Kibler, B. *et al*. The Peregrine soliton in nonlinear fibre optics. *Nature Phys.* **6**, 790–795 (2010).
14. Schouten, H. F., Visser, T. D., Lenstra, D. & Block, H. Light transmission through a subwavelength slit: Waveguiding and optical vortices. *Phys. Rev. E* **67**, 036608 (2003).
15. Manton, N. S. & Sutcliffe, P. Topological Solitons (Cambridge University Press 2004).
16. Dennis, M. R., O'Holleran, K. & Padgett, M. J. Singular Optics: Optical Vortices and Polarization Singularities. *Progr. in Optics* **53**, 293–363 (2009).
17. Soskin, M. S. & Vasnetsov, M. V. Singular Optics. *Progr. in Optics* **4**, 219–276 (2001).
18. Rozanov, N. N. Formation of radiation with wave – front dislocations. *Opt. Spectrosc.* **75**, 861–867 (1993).
19. Gregg, P., Kristensen, P. & Ramachandran, S. Conservation of orbital angular momentum in air-core optical fibres. *Optica* **2**, 267–270 (2015).
20. Milonni, P. W. & Boyd, R. W. Momentum of Light in a Dielectric Medium. *Adv. Opt. Photon.* **2**, 519–553 (2010).
21. Picardi, M. F., Bliokh, K. Y., Rodriguez – Fortuno, F. J., Alpeggiani, F. & Nori, F. Angular momenta, helicity, and other properties of dielectric – fibre and metallic – wire modes. *Optica* **5**, 1016–1026 (2018).
22. Bozinovic, N. *et al*. Terabit-Scale Orbital Angular Momentum Mode Division Multiplexing in Fibres. *Science* **340**, 1545 (2013).
23. Willner, A. E. *et al*. Optical communications using orbital angular momentum beams. *Adv. Opt. Photon.* **7**, 66–106 (2015).
24. Ferrando, A., Zacares, M., Fernandez de Cordoba, P., Binosi, D. & Monsoriu, J. A. Vortex solitons in photonic crystal fibres. *Opt. Express* **12**, 817–822 (2004).
25. Dong, S. L. & El – Hang, L. Structural characteristics and properties of phase singularities in optical fibres. *Journ. Opt. Soc. Korea* **1**, 81–89 (1997).
26. Alexeyev, C. N., Fadeyeva, T. A., Volyar, A. V. & Soskin, M. S. Optical vortices and flow of their angular momentum in a multimode fibre. *Quantum Electronics & Optoelectronics* **1**, 82–89 (1998).
27. Alexeyev, C. N., Volyar, A. V. & Yavorsky, M. A. Linear azimuthons in circular fibre arrays and optical angular momentum of discrete optical vortices. *Phys. Rev. A* **80**, 063821 (2009).
28. Berry, M. V. Optical currents. *J. Opt. A: Pure Appl. Opt.* **11**, 094001 (2009).
29. Bekshaev, A., Bliokh, K. Y. & Soskin, M. Internal flows and energy circulation in light beams. *J. Opt.* **13**, 053001 (2011).
30. Novitsky, A. V. & Barkovsky, L. M. Poynting singularities in optical dynamic systems. *Phys. Rev. A* **79**, 033821 (2009).
31. Novitsky, A. V. & Novitsky, D. V. Negative propagation of vector Bessel beams. *JOSA A* **24**, 2844–2849 (2007).
32. Luan, F. *et al*. All – solid band gap fibres. *Opt. Lett.* **29**, 2369–2371 (2004).
33. Pryamikov, A. D. *et al*. Demonstration of a waveguide regime for a silica hollow – core microstructured optical fibre with a negative curvature of the core boundary in the spectral region > 3.5 μm. *Opt. Express* **19**, 1441–1448 (2011).
34. Wang, Y. Y., Wheeler, N. V., Couny, F., Roberts, P. J. & Benabid, F. Low loss broadband transmission in hypocycloid – core Kagome hollow – core photonic crystal fibre. *Opt. Lett.* **36**, 669–671 (2011).
35. Fei, Y., Wadsworth, J. & Knight, J. C. Low loss silica hollow core fibres for 3 – 4 μm spectral region. *Opt. Express* **20**, 11153–11158 (2012).
36. Pryamikov, A. D. & Alagashev, G. K. Features of light leakage from the negative curvature hollow core fibres. *Opt. Engineering* **57**, 066106 (2018).
37. Baranova, N. B. & Zeldovich, D. Ya. Dislocations of the wave – front surface and zeros of the amplitudes. *Sov. Phys. JETP* **53**, 925–929 (1982).
38. Volyar, A. V. & Fadeeva, T. A. Angular momentum of the fields of a few – mode fiber: I. A perturbed optical vortex. *Tech. Phys. Lett.* **23**, 848–851 (1997).
39. Kolyadin, A. N. *et al*. Light transmission in negative curvature hollow core fibre in extremely high material loss region. *Opt. Express* **21**, 9514–9519 (2013).
40. White, T. P. *et al*. Multipole method for microstructured optical fibres. *JOSA B* **19**, 2322–2330 (2002).
41. Snyder, A. W. & Love, J. D. Optical waveguide theory (Chapman and Hall, London New York).
42. Pryamikov, A. D. & Alagashev, G. K. Strong light localization and a peculiar features of light leakage in the negative curvature hollow core fibers. *Fibers* **5**, 43–54 (2017).

43. Vasnetsov, M. V., Gorshkov, V. N., Marienko, I. G. & Soskin, M. S. Wavefront motion in the vicinity of a phase dislocation: "Optical Vortex". *Opt. Spectrosc.* **88**, 260–265 (2000).
44. Litchinitser, N. M., Abeeluck, A. K., Headley, C. & Eggleton, B. J. Antiresonant reflecting photonic crystal optical waveguides. *Opt. Lett.* **27**, 1592–1594 (2002).
45. Alagashev, G. K. *et al*. Impact of geometrical parameters on the optical properties of negative curvature hollow core fibres. *Laser Phys.* **25**, 055101 (2015).
46. Pryamikov, A. D., Alagashev, G. K., Kosolapov, A. F. & Biriukov, A. S. Impact of core – cladding boundary shape on the waveguide properties of hollow core microstructured fibres. *Laser Phys.* **26**, 125104 (2016).
47. Jaison, G. T., Richardson, D. J. & Poletti, F. Novel anti-resonant hollow core fiber design with ultralow leakage loss using transverse power flow analysis. Th3E.2, OFC 2019.

Acknowledgements

The work of SKT was supported by the Russian Science Foundation (Grant No. 17–72–30006). The work of A.P. and G.A. was supported by the Russian Science Foundation (Grant No. 18-19-00733).

Author contributions

A.P. initiated the study and supervised the numerical modeling. G.A. conducted the numerical modeling and analyzed the data. A.P., G.F. and S.T. analyzed the data and wrote the paper.

Competing interests

The authors declare no competing interests.

Additional information

Correspondence and requests for materials should be addressed to A.P.

Reprints and permissions information is available at www.nature.com/reprints.

Publisher's note Springer Nature remains neutral with regard to jurisdictional claims in published maps and institutional affiliations.